Received 6 August 2023; revised 27 October 2023; accepted 10 November 2023. Date of publication 15 November 2023; date of current version 30 January 2024.

Digital Object Identifier 10.1109/OJAP.2023.3333226

On Performance Characterization of Harmonic Transponders

MILAN POLIVKA [1] (Member, IEEE), AND JEFF FROLIK [2] (Senior Member, IEEE)

[1]Faculty of Electrical Engineering, Czech Technical University, 166 36 Prague, Czechia

[2]Department of Electrical and Biomedical Engineering, University of Vermont, Burlington, VT 05405, USA

CORRESPONDING AUTHOR: J. FROLIK (e-mail: jfrolik@uvm.edu)

This work was supported in part by the Czech Science Foundation under Grant GA23-07518S; in part by the U.S. Bureau of Educational and Cultural Affairs under Grant 12155-EZ; and in part by the USDA National Institute of Food and Agriculture under Grant 2023-67022-38830.

ABSTRACT Harmonic transponders are passive wireless devices that hold great promise for a variety of long-term tracking and sensing applications. These nonlinear devices receive an interrogation signal at one frequency (f) and backscatter harmonics (typically, $2f$ is of interest). The device's conversion loss is the change in power from what is received and what is transmitted. We show herein that conversion loss is dependent jointly on interrogation power, interrogation frequency, and interrogation angle. This coupled nature of the device's behavior necessitates performance metrics that capture these characteristics. We present a methodology to generically test these devices and propose metrics that capture the noted dependencies.

INDEX TERMS Backscatter, conversion loss, dual band, frequency doubler, harmonic transponder, metrics, nonlinear circuits, patch antennas, over-the-air testing, RFID, wireless sensor.

I. INTRODUCTION

WIRELESS sensors are a means by which we can better monitor, and thus better understand, both natural and built environments, and in a manner that is less intrusive and less costly than wired approaches. For many applications, sensors may need to be deployed for extended periods of time (e.g., years) and/or in environments where battery replacement is not tenable (e.g., within a media and/or where hazards exist). For such applications, *passive* wireless sensors are a promising solution.

Harmonic transponders are one such passive wireless device, an example shown in Fig. 1-*Top*, and which have been investigated for a variety of novel identification and sensing purposes, including tracking of insects [1], [2], [3], [4]; avoiding car collisions [5]; locating buried infrastructure [6]; monitoring steel corrosion [7], wall cracks [8], and railbeds [9]; and measuring temperature [10], [11], [12], humidity [13], and soil moisture [14]. As illustrated in Fig. 1-*Bottom*, harmonic transponders are nonlinear devices, which operate by receiving an interrogation signal at one frequency (f) and returning its harmonics (typically, $2f$ is of interest, since it is usually the strongest return). The response at a different frequency (i.e., $2f$ versus f) is considered a key advantage over transponders operating on a single frequency (e.g., RFIDs), as it avoids self-jamming and uniquely identifies a transponder's response from reflections in high clutter environments [15].

While scattering from non-linear devices has been described since the 1970s (e.g., [5], [17]), often in terms of "harmonic radar", to date, the research community has not firmly established metrics by which the performance of various transponder designs might be assessed and compared. A key parameter that will dictate the effectiveness of a particular harmonic transponder design, and consequently the performance of the whole system, is the device's overall *conversion loss* (CL), which is the ratio of the power incident at the harmonic transponder's receive antenna (at f) to the power of the harmonic backscattered from its transmit antenna (e.g., at $2f$). As these devices are nonlinear, the conversion loss is a function of incident power at the device's diode. As this incident power will depend on the device's receive antenna pattern, the conversion loss is also

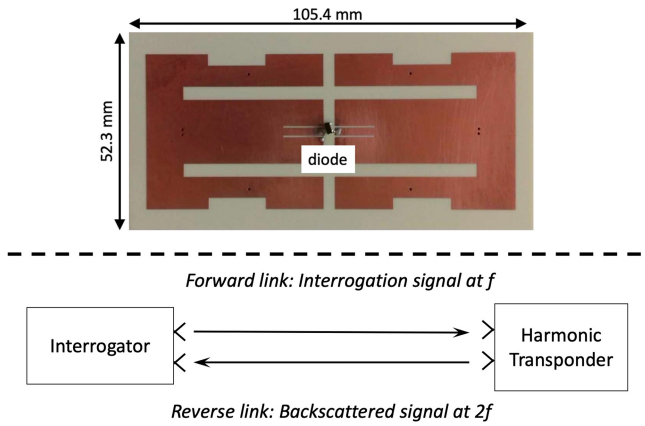

FIGURE 1. ***Top*: Harmonic transponder design leveraged in this work, previously presented in [16]. *Bottom*: Wireless interrogation of a harmonic transponder at *f*, where the return signal of interest is at the second harmonic (2*f*).**

a function of direction. Finally, harmonic transponders are resonant devices, with complex antenna impedances having steep imaginary slopes at their operating frequencies [16]. As such, conversion losses are also frequency dependent. Thus to fully characterize the performance of a harmonic transponder, *CL* should be understood across the three dimensions of power, frequency, and interrogation angle.

To date, only a few studies have seek to characterize harmonic transponder performance, analytically and experimentally [18], [19], [20] at the *device-level* (i.e., after the transponder has been fully integrated). Even fewer (e.g., [19]) also consider the directional characteristics of transponders. From these works, we can begin to glean what might be suitable metrics for characterizing a harmonic transponder's performance.

Analytical models for the harmonic response of diode-based transponders, based on equivalent circuit models of antenna-diode junctions, were derived in [18] and [20]. Both works considered a SPICE model of the diode, the parasitic elements of its package, and a series model for antenna input impedances. In [18], the resulting expression for the conversion loss is separated in two terms. The first term, $\mathrm{FOM_a}$, is the figure-of-merit for the antenna and describes the power transmission through the antenna-diode interface including the antenna's radiation efficiency.[1] The second term, $\mathrm{FOM_{diode}}$, is the figure-of-merit for the diode and describes conversion efficiency of the diode P-N junction. This term is expressed as a function of the antenna quality factor (Q_a). As Q_a of a real antenna is calculated from charge/current distributions or derived from the input impedance waveform, using frequency derivatives [21], and/or estimated from the bandwidth, it is not clear to the authors as to this metric's practicality.

The other work, [20], similarly expressed the conversion efficiency/loss, showing the relationship between the diode's SPICE parameters and the conversion loss to identify suitable diode(s) with the lowest *CL*. Both of these works considered different power levels incident on the transponder to show the change in *CL* over power, however they did not consider frequency and spatial dependency of *CL* caused by narrowband behavior and directional characteristics of the antenna, both which we show herein significantly affect the overall transponder performance.

Herein, we both propose metrics that capture a harmonic transponder's conversion loss performance over the triplet of power, frequency and direction and present a methodology for collecting the data for these metrics. While we illustrate our methodology using purely passive harmonic transponders, the approach is generally applicable to designs where voltage biases influence device conversion loss (e.g., [22], [23]).

In Section II, we review an earlier presented FOM, that relates a harmonic transponders performance to the distance it can be detected. This FOM is limited in its practicality, and therefore in Section III we presented strategies to collect data that allows fuller characterization of these devices. In Section IV, we apply the proposed strategies to the dual-band patch-type antenna device seen in Fig. 1. Based on these results, we present in Section V several possible performance metrics that will allow researchers and practitioners to readily compare designs. Section VI provides our concluding remarks.

II. AN EXISTING PERFORMANCE METRIC

As noted, the harmonic transponder's conversion loss is the parameter that expresses the efficiency of power conversion between interrogation signal, at frequency f, and the backscattered signal, at $2f$. Thus this parameter directly affects the bidirectional radio link budget and any link margins of interest. Fig. 2 presents the link parameters which will determine, e.g., the received backscattered power for a given interrogation power.

The signal transmitted by the interrogator, at f, will be at a particular power (P_{tx}) and sent with an antenna having particular gain ($G_{tx,f}$). The backscattered signal, at $2f$, will be received by the interrogator using an antenna having particular gain ($G_{rx,2f}$) and will have a measured power (P_{rx}). The conversion loss of the harmonic transponder is determined by its receive antenna gain ($G_{ht,f}$) at f, its transmit antenna gain ($G_{ht,2f}$) at $2f$, and finally the transponder's diode conversion loss (CL_d). Assuming *free-space* conditions [24], the forward (FPL_f) and reverse (FPL_r) path losses for the link can be found through the Friis equation (as is illustrated in the Appendix).

However, perhaps of greatest interest to the user of a harmonic transponder is its *read range*, i.e., at what distance can the device be interrogated. With this practicality in mind, [20] presented the metric *"maximum" detection range*.[2]

1. However, $\mathrm{FOM_a}$ does not correspond exactly to the transmission coefficient across the antenna-diode interface.

2. We qualify "maximum" as this metric is defined using very specific system parameters, details discussed shortly.

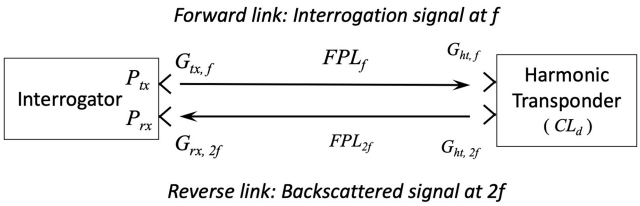

FIGURE 2. Harmonic transponder bidirectional link.

This metric is found using the link parameters shown in Fig. 2 to calculate, first, the range of the forward link (d_1), then that of the reverse link (d_2), and finally the figure of merit (FOM$_d$) as the mean of those values, per the equations below.[3]

$$\text{FOM}_d = \frac{d_1 + d_2}{2} \tag{1}$$

where

$$d_1 = \frac{\lambda}{4\pi \times 10^{-(P_{tx}+G_{tx,f}+25+G_{ht,f})/20}}$$

and

$$d_2 = \frac{\lambda/2}{4\pi \times 10^{-(75-CL_d+G_{ht,2f}+G_{rx,2f})/20}}$$

The calculation of d_1 is for a specific link condition, when the interrogator's EIRP (effective isotropic radiated power) is 35 dBm and the power incident *at the diode* is −25 dBm. The d_2 calculation is performed for the specified receiver sensitivity threshold of $P_{rx} = -100$ dBm ($G_{rx,2f}$ of 10 dBi is assumed). Under these very prescribed conditions, FOM$_d$ provided a metric by which the performance of transponder designs from different research groups were compared [20, Table III].

This metric was also applied by the authors to their own recently presented design [16],[4] and due in part to their device's asymmetric antenna gains, lead to $d_1 = 32.2$ m, a significantly larger $d_2 = 144.7$ m, and a FOM$_d = 88.4$ m. Similar disproportions were presented in [20] for devices developed in [8] ($d_1 = 10.0$ m, $d_2 = 4.1$ m) and in [13] ($d_1 = 8.2$ m, $d_2 = 2.6$ m).

As conversion loss is a nonlinear function of incident power, under asymmetric links conditions such as these, we contend the physical meaning of averaging of d_1 and d_2 is not evident. We also observe that impedance mismatching terms corresponding to the antenna-diode interfaces are not explicitly considered in Eq. (1), or was it noted to be included in the transponder antenna gains. As such, we are motivated to find more intuitive and generally applicable metrics, with clearer physical meanings.

3. The various link terms in these equations are in log form, i.e., in dB, dBi, dBm.

4. In [16], the d_1 was calculated in error using EIRP of 25 dBm, resulting in $d_1 = 10.2$ m.

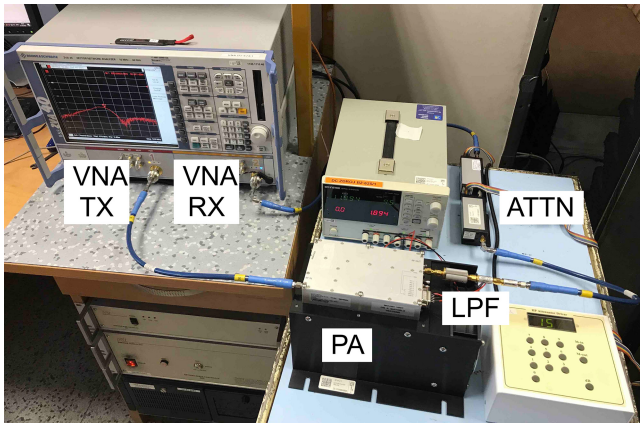

FIGURE 3. VNA with external hardware and showing example measurement data.

III. MEASUREMENT APPROACH

Our recent work has shown that the conversion loss of a harmonic transponder also varies *jointly* with power *and* frequency [25]. In addition, as harmonic transponders have both receive and transmit antennas (either two separate elements, as in [13], [20], [26], or with a single dual-band design, as in [16]), their conversion loss will also be affected by their directional characteristics, i.e., by the angle at which they are interrogated. In short, a metric such as provided in Eq. (1), which considers a *fixed* frequency, interrogation power and/or angle of interrogation, does not fully capture the performance characteristics of harmonic transponders. In this section, we propose a measurement approach to fully characterize harmonic transponders, which allowed us to obtain the results presented in Section IV.

Our test setup (Fig. 3) employed a laboratory grade, two-port vector network analyzer (VNA - Rohde & Schwarz ZVA 40), followed by a power amplifier (PA - MiniCircuits ZHL-4W-422+), two low pass filters (VLF-1200+, MiniCircuits), and then two switchable attenuators (HP 84904L and 84906L), which enabled testing over a 40 dB dynamic range of incident powers, while not introducing any nonlinearities in the test setup.

Harmonic transponders were tested in an anechoic chamber using linearly-polarized antennas (RFspin QRH11: $G_{tx,f} = 4.8$ dBi, $G_{rx,2f} = 7.4$ dBi [27]), which were spaced 0.44 m apart (Fig. 4). Transmit and receive links lengths were each 2 m. Testing was conducted to collect azimuth (H-plane, yz) patterns with EIRP values from +32.2 dBm to −2.8 dBm, which corresponds to power incident at the transponder from −5 dBm to −40 dBm, respectively. Each measurement swept the interrogation frequency from 870 MHz to 910 MHz and synchronously measured the backscattered signal from 1740 MHz to 1820 MHz.

Ascertaining CL from measured data is readily found using the following link budget equation[3]

$$CL = P_{tx} - P_{rx} + G_{tx,f} + G_{rx,2f} - FSL_f - FSL_{2f}, \tag{2}$$

where the free space losses at f (FSL_f) and $2f$ (FSL_{2f}) are found from Eqs. (8) and (9) of the Appendix, respectively,

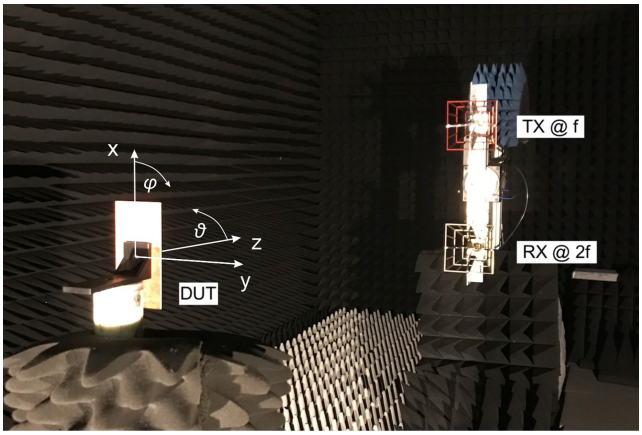

FIGURE 4. Bistatic, anechoic chamber test setup. Link length: 2 m. Radiation pattern measured in H-plane (*yz*).

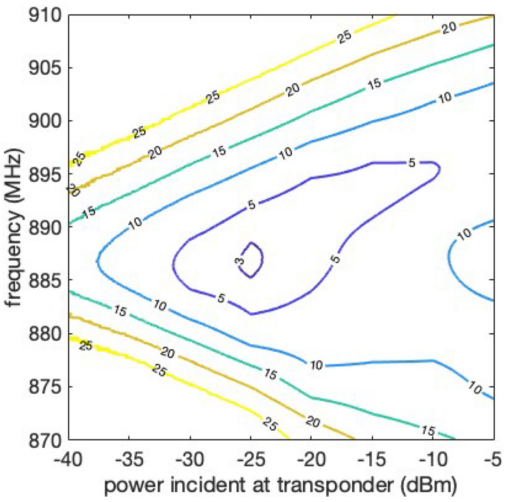

FIGURE 5. Transponder conversion loss (dB) for normal incidence case over frequency and incident power. Data illustrates (i) narrowing of response bandwidth with decreased incident power at the device and (ii) frequency shifting with increased power. The minimum device conversion loss is 2.75 dB.

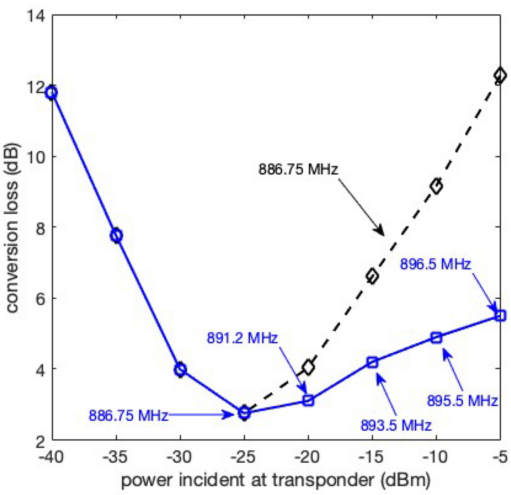

FIGURE 6. Transponder conversion loss (*CL*) for normal incidence case over power incident at the device. As incident power exceeds that which achieves the lowest conversion loss (i.e., −25 dBm), the device "detunes" from 886.75 MHz (dashed) to achieve lowest *CL* at increasingly higher frequencies (solid).

and the link distance for the test setup (e.g., 2 m in our case).

Note that this testing leveraged a high-end two-port VNA, which is able to synchronously transmit (Port 1) and receive (Port 2) in different frequency bands (i.e., f and $2f$, respectively). This capability is not found in all VNAs, particularly portable instruments that may be used for field testing. As such, the authors would like to refer the reader to an alternative approach that leverages any two-port VNA, along with a $\div 2$ frequency divider circuit, and which provides comparable measurement results [25].

IV. CONVERSION LOSS DEPENDENCIES

One objective of this work is to present methods that can be broadly applied by researchers, so that different harmonic transponder designs can be readily compared. Data is presented here that were obtained using the test setup and procedure described in the prior section. For illustrative purposes, measurements were made for the harmonic transponder shown in Fig. 1. This transponder is composed of a dual-band patch-type antenna, loaded by an HSMS-2820 Schottky diode. The author's prior work [16] details its design and the rationale for this diode choice. The conversion loss dependencies presented below are used to motivate the performance metrics proposed in the next section.

A. CONVERSION LOSS OVER FREQUENCY AND POWER

We begin by illustrating the joint response over incident power and interrogation frequency. With the harmonic transponder oriented normal to the interrogator (i.e., $\theta = 0°$, $\phi = 0°$), P_{rx} data was collected from 870 MHz to 910 MHz at eight incident power levels (−40 dBm to −5 dBm, in 5 dB increments). From these data, device *CL* was calculated using Eq. (2) and is presented in Fig. 5.

The minimum conversion loss was found to be 2.75 dB at a frequency of 886.75 MHz, when the incident power at the device was −25 dBm. As the power is decreased, the conversion loss is seen to increase (as expected) and in a manner that is symmetric in frequency. At the same time, the response bandwidth narrows. However, when the incident power is increased relative to −25 dBm, we note a distinct positive frequency shift in the resonant frequency. For instance, when the incident power is increased by 20 dB to −5 dBm, this shift is nearly 10 MHz (to 896.45 MHz). To see this effect more clearly, we present Fig. 6, which shows the conversion loss versus incident power for a fixed frequency (886.75 MHz), along with the minimum conversion loss seen across all frequencies. This "detuning" is the result of the diode being operating in its large signal region (i.e., $P_{in} > -20$ dBm [28]), which causes its input impedance to change significantly.

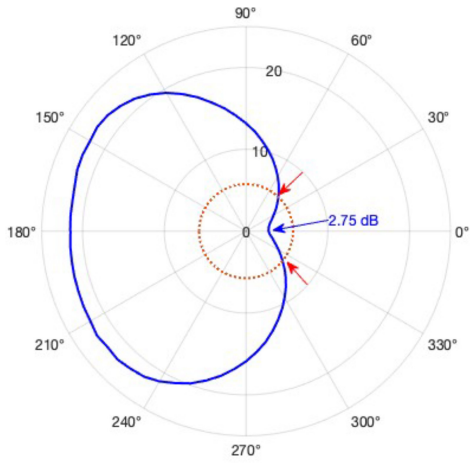

FIGURE 7. Example directional conversion loss (dB) over azimuth angle ($\phi = 0°$). This particular curve illustrates the minimum transponder conversion loss (2.75 dB) measured over all frequencies and incident powers, specifically at 886.75 MHz and −25 dBm. In addition, the 3 dB beamwidth is shown to be ∼90°.

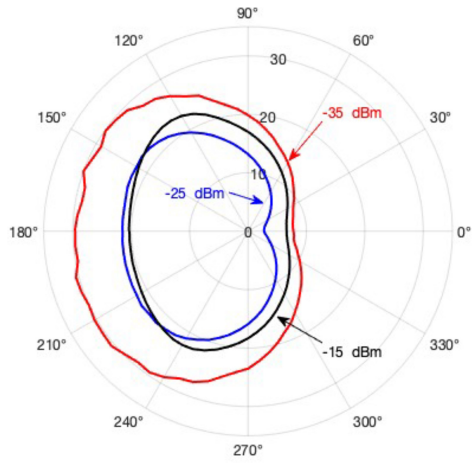

FIGURE 8. Transponder conversion loss (dB) versus azimuth angle and across a 20 dB dynamic range of incident powers: −15 dBm, −25 dBm (as also seen in Fig. 7), and −35 dBm.

B. CONVERSION LOSS VERSUS DEVICE ORIENTATION

The third dimension we explore is the orientation of a harmonic transponder. We limit our presentation to azimuth (H-plane) characterization, but the approach can be generalized to elevation (E-plane) cuts and full 3D mapping.

Fig. 7 presents azimuth data (360° at 5° increments) at 886.75 MHz for an incident power at the transponder of −25 dBm (i.e., the conditions of interrogation frequency and incident power found in Fig. 5 to yield the minimum conversion loss). Notable from this figure is that the pattern encompasses (*i*) the directivity changes in the transponder's receive antenna operating at f, (*ii*) the directivity changes in the transponder's transmit antenna at $2f$, *and* (*iii*) the nonlinearity in conversion losses as the incident power at the diode changes with angle. This measurement scenario differs from that presented in [19], where that approach maintained the incident power at the diode so as to map *only* the radiation pattern of the transponder's transmit antenna, not the full device.

As expected for a patch-type design, the device's antennas have peak gain in the normal direction, therefore this direction also shows the minimum conversion loss.[5] For additional context, we provide a contour for which the conversion loss has increased 3 dB relative to the minimum of 2.75 dB. For this particular harmonic transponder, there is ∼90° 3 dB conversion loss beamwidth, when the normal incident power is −25 dBm. This directional measure could be relevant for applications in which transponders are placed on objects for tracking purposes.

To illustrate the effects of incident power, we show in Fig. 8 azimuth radiation cuts over a 20 dB dynamic range. We note significant change, not only in the magnitude of the conversion loss over the three different cases, but also in the shape of the radiation pattern. As the transponder's receive and transmit antenna radiation patterns are power independent, these changes are due solely the diode's nonlinearity and detuning effects.

V. PROPOSED PERFORMANCE METRICS

As noted that the onset of this work, to date, performance metrics for harmonic transponders are few and those that have been proposed are limited to constrained scenarios, which limit their practical use. We have also shown that a device's conversion loss is highly dependent on interrogation frequency, incident power, and interrogation angle. In this section, we endeavor to provide metrics that are both meaningful in practice and capture a harmonic transponder's multifaceted behavior.

A. EXPECTED FREE SPACE READ RANGE

We now provide what we believe is an improved FOM, which we refer to as the *expected free space read range*, d_r, as given by Eq. (3),[6]

$$d_r = \frac{\lambda}{4\pi \times 10^{-C/40}} \tag{3}$$

where the term C is given by Eq. (4)[3]

$$C = P_{tx} - P_{rx} + G_{tx,f} + G_{rx,2f} - CL - 6. \tag{4}$$

P_{tx} is the power delivered at the antenna input connector, which includes cable losses at f and any power amplifier gain. Similarly, P_{rx} will include cable losses at $2f$. CL is the conversion loss of the harmonic transponder *as a whole*, which includes the gains of its receive and transmit antenna ($G_{ht,f}$ and $G_{ht,2f}$, respectively), diode conversion loss (CL_d), and antenna-diode impedance mismatching ($L_{m,f}$, $L_{m,2f}$), as we capture in Eq. (5)[3]

$$CL = CL_d + L_{m,f} + L_{m,2f} - G_{ht,f} - G_{ht,2f}. \tag{5}$$

5. For details on the radiation patterns for this transponder's dual-band patch antenna, please see [16].

6. For the complete derivation of Eq. (3), please see the Appendix.

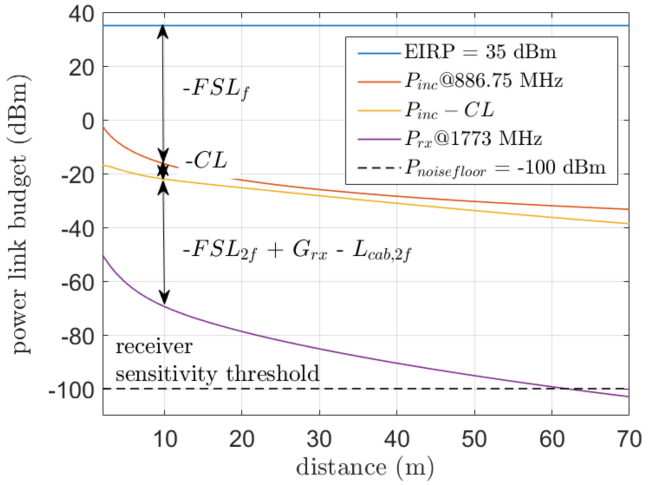

FIGURE 9. Free space read range (d_r) for the harmonic transponder seen in Fig. 1, under the EIRP (35 dBm) and P_{rx} (−100 dBm) constraints specified in [20]. The expected free space read range of 62 m is achieved at 886.75 MHz and in the direction normal to the device.

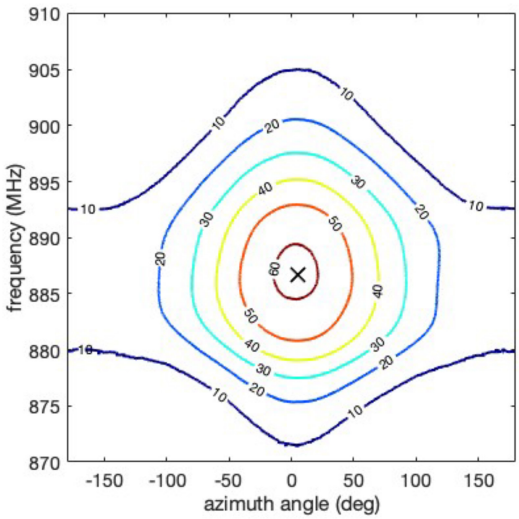

FIGURE 10. Expected free space read range (m) for the harmonic transponder seen in Fig. 1 over azimuth angle (H-plane) and under the EIRP and P_{rx} constraints specified in [20]. "×" marks maximum d_r of 62 m.

This metric differs from FOM_d, given by Eq. (1), in that it captures, in one expression, the *bidirectional* free space link losses. Furthermore, it removes the constraints on upon which Eq. (1) is based, i.e., that (i) EIRP = 35 dBm, (ii) $P_{\text{inc\_diode}} = -25$ dBm, (iii) $P_{rx} = -100$ dBm, and (iv) $G_{rx,2f} = 10$ dBi. Eq. (3) also accounts for, in an intuitive manner, any imbalance that may exist between the forward and reverse interrogation links (recall the discussion regarding the impact of wildly different d_1 and d_2 on the calculation of FOM_d). An additional advantages of this proposed metric is that unknowns such as antenna diode mismatch or radar cross section (RCS) [29], or those associated with integrating the harmonic transponder's components, are captured at the device level.

Because a diode is a non-linear device, its conversion loss (CL_d), will be dependent on the power incident on the device, which is dependent on the read distance, d_r. As such, solving for d_r does require knowledge of CL over power (e.g., as seen in Fig. 6) and is an iterative process, which we outline in the Appendix.

As described in detail in Section III, CL can be found experimentally using short range testing. Once this data is obtained, C, and subsequently d_r, for a particular scenario can be found, from Eqs. (4) and (3), respectively. Using our empirical data collected at 2 m, the calculation presented in Eq. (3), and, for comparison purposes, *some* the constraints for the metric FOM_d (i.e., EIRP = 35 dBm and $G_{rx,2f} = 10$ dBi), we plot in Fig. 9 the expected power received as a function of link distance. For the threshold of $P_{rx} = -100$ dBm specified in [20], we find an expected free space read range of 62 m. We note that this read range is achieved when $P_{\text{inc\_diode}} = -32.25$ dBm, versus the −25 dBm specified by FOM_d. We also note that the expected free space read range, under such posed constraints, does not necessarily correspond to the device operating at its minimum CL. For instance, the d_r presented in Figs. 9 and 10 has the device $CL = 4.5$ dB (vs. its minimum of 2.75 dB), as seen in data tips of Fig. 9.

The impact of interrogation frequency and device orientation on the read range is illustrated in Fig. 10. As expected, the read range will decrease both as the device is interrogated at suboptimal frequencies and non-normal angles. The rate of this decrease will be dependent on the device's antennas and tuning and is, for practical applications, useful to know.

While the problem of calculating read range based on fixed system parameters is useful to compare the relative performance of different harmonic transponders, we contend the true benefit of Eq. (3) is for designing the system itself. That is, given a transponder and desired read range, transmitter powers, antennas, and receiver sensitivities can all be specified.

B. OTHER USEFUL MEASURES

While the proposed expected free space read range metric, d_r, obtained from Eq. (3), provides values consistent with our empirical results, it *still* requires a specified EIRP, P_{rx}, etc., in order to compare across different designs. Furthermore, this read range metric does not account for realistic non-free space applications, such as when harmonic transponders are located in a cluttered environment and/or mounted in/on an object. As such, perhaps a more useful strategy is to remove all aspects of how the device is interrogated and channel effects, and simply provide its fundamental performance parameters. We suggest that the following data can provided.

- CL_{min}: From data measured, what is the minimum conversion loss noted.
- The incident power *at the device*, along with the frequency, for which CL_{min} was obtained.

These data can then be plotted as illustrated in Fig. 11 and in which we compare the harmonic transponder seen

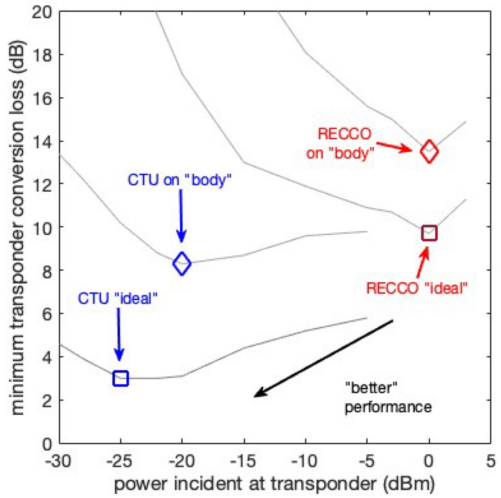

FIGURE 11. Proposed metric for harmonic transponder comparisons: Minimum conversion loss (CL_{min}) vs. incident power at device at which CL_{min} is achieved. The metric is used here to compare two devices (CTU and RECCO), at two different frequencies (886.75 MHz and 890 MHz, respectively), and under two different implementation scenarios (on "body" and under "ideal" anechoic conditions). Light lines show the measured *CL* over a range of incident powers.

in Fig. 1 (CTU), with a commercially available avalanche reflector (RECCO) [30]. We note that these measured data allow us to compare devices operating in different bands as the data for the CTU device was collected at 886.75 MHz, while at 890 MHz for the RECCO reflector. As the RECCO reflector has an omnidirectional, dipole antenna design, it is not unexpected that its minimum *device-level* conversion loss would be greater than our directional patch antenna design. We also show the impact of placing these devices near a human body phantom of oval cylinder shape (160 × 120 × 80 mm, $\epsilon_r = 60$ & $\sigma = 2.5$ S/m), the subject of our complementary work [31].

To understand the measured reduction in device performance when placed on a body, an analysis using CST Studio Suite EM simulator was conducted, which showed that both the directivity and radiation efficiency of the CTU transponder's dualband antenna degrade. The degradation is especially noted at the fundamental frequency, for which the ground plate is relatively small compared to the wavelength. The simulated total degradation for the CTU device was found to be 4.75 dB, which corresponds to the measured difference between conversion losses for 'ideal" and "body" cases in Fig. 10, and the increased power required to achieve the minimum *CL*.

We have seen that CL_{min} will be achieved at a particular frequency and at a particular orientation of the transponder. From Figs. 5 and 7, the conversion loss will degrade as one moves away from this frequency and/or orientation. As such, perhaps of additional importance would be to know the following metrics.

- *3 dB bandwidth:* The frequency range over which the *CL* is within 3 dB of CL_{min}. From the data presented Fig. 5, this value was found to be ∼11.15 MHz.
- *3 dB beamwidth:* The beamwidth for which the *CL* is within 3 dB of CL_{min}. As illustrated by the red arrows in Fig. 7, for our device, this value is ∼90°.

With these four metrics, one could readily design a *system*, consisting of harmonic transponders *and* an interrogator, based on operational constraints for read range, maximum EIRP, receiver sensitivity, coverage area, etc.

C. COMBINED TRANSMISSION COEFFICIENT

To conclude this work, we present one final metric that we contend is useful for the design of a harmonic transponder. As noted, our measured data indicates frequency dependency in the transponder's conversion loss. We reconsider the author's prior work and data ([16, Fig. 9]) for the harmonic transponder seen in Fig. 1. Fig. 12 - Top shows the transmission coefficient, T, found between the transponder's dualband antenna and the diode impedances. The device's overall conversion loss is greatly impacted by T, whose response is shown here to be extremely narrowband, due to the steep slope of the imaginary part of the antenna impedance at both operating frequencies. In Fig. 12 - Bottom, we show the combined (dualband) transmission, T_{comb}, over the impedance interface, which covers both operating bands simultaneously. This figure represents the total mismatch loss (dB), which is defined as the sum of the transmission coefficients of both operating bands

$$T_{\text{comb}}(f_i) = T(f_i) + T(2f_i), \tag{6}$$

and where the indices $i = 1, \ldots, N$ represent the sample series in each frequency band.

We note that there is good impedance matching at the upper operating frequency (f_2) and worse matching at the lower frequency ($f_1 = f_2/2$), which results in degraded combined matching value at the design's targeted pair of frequencies, i.e., 894 MHz and 1788 MHz, and a better value at a slightly different frequency pair ($f_1 - df =$ 888 MHz, $f_2 - 2df =$ 1776 MHz). To our knowledge, the combined transmission, T_{comb}, has not been studied during the development process of harmonic transponders. Considering this metric will likely improve the prediction of the harmonic transponder's true performance.

VI. CONCLUSION

In this work, we have endeavored to make the case that intuitive metrics, with clear physical meanings, for characterizing harmonic transponder performance are needed. We demonstrated that these non-linear, frequency-dependent, directional devices have conversion loss behaviors which are jointly dependent on these three parameters. As such, to fully characterize devices, a single power/frequency/directional point measurement will not suffice. We present a methodology for collecting the requisite data, along with simple, intuitive metrics we hope will allow various designs to be compared.

These metrics can reveal inherent transponder behaviour, which will directly affect the functional parameters of the

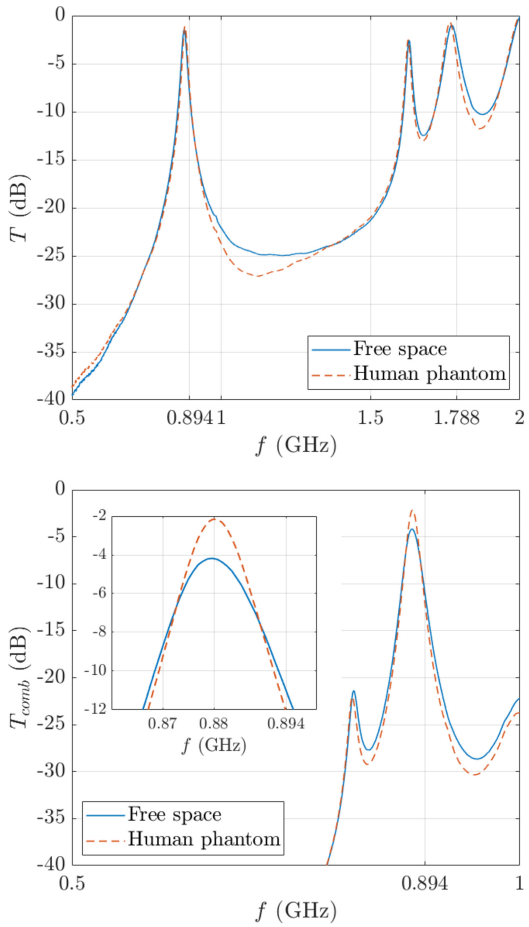

FIGURE 12. Top: Transmission coefficient (in dB) of antenna-diode impedance interface covering both lower (fundamental) and upper (second harmonic) frequency bands; taken from [15]. Bottom: Combined (dualband) transmission coefficient, reference to the lower band. The detail view shows that the maximum dualband transmission is shifted to 888 MHz, from the forward only transmission peak of 894 MHz.

interrogator. For example, to determine the distance of a transponder, an interrogator may need to sweep quickly across a frequency band and at various powers to ensure the embedded transponders response is characterized before the distance can be calculated from the received power. This problem becomes significantly more complex when the channel is not free space, i.e., the device is embedded in a cluttered or lossy channel.

In addition, our results indicate that the modeling needed to predict the performance of harmonic transponders needs to be advanced beyond the present approach of separately considering antenna and diode behaviors or considering performance at only a fixed frequency and/or fixed incident power. In short, there are still open issues related to the characterization of harmonic transponders used for tracking and sensing. Our hope is that this work helps in this effort by providing metrics for quantifying performance.

APPENDIX
DERIVATION OF EQ. (3)

We begin by writing the non-log form of the *bidirectional* link equation for the harmonic transponder system, which is based on the Friis transmission formula that includes the transponder conversion loss (CL). This equation has been used by others (e.g., [32]) to estimate the power received at the interrogator for a particular link configuration.

$$P_{rx} = \frac{P_{tx} \times G_{tx} \times G_{rx}}{FSL_f \times CL \times FSL_{2f}} \tag{7}$$

The forward link (at frequency f) and reverse link (at frequency $2f$) free space losses, FSL_f and FSL_{2f}, respectively, for a distance r are given by the following,

$$FSL_f = \left(\frac{4\pi r}{\lambda}\right)^2 \tag{8}$$

and

$$FSL_{2f} = \left(\frac{4\pi r}{\lambda/2}\right)^2, \tag{9}$$

as the frequency of interest on the reverse link is twice that of the forward link. The bidirectional, free space link loss, FSL_b, becomes the product of these individual losses.

$$FSL_b = FSL_f \times FSL_{2f} = 4 \times \left(\frac{4\pi r}{\lambda}\right)^4$$

We can now rewrite Eq. (7) to solve for this loss,

$$FSL_b = 4 \times \left(\frac{4\pi r}{\lambda}\right)^4 = \frac{P_{tx} \times G_{tx} \times G_{rx}}{P_{rx} \times CL}$$

from which we can determine the *expected free space read range*, $r = d_r$, if the interrogator parameters (P_{tx}, P_{rx}, G_{tx} and G_{rx}) are known.

$$d_r = \frac{\lambda}{4\pi} \sqrt[4]{\frac{P_{tx} \times G_{tx} \times G_{rx}}{4 \times P_{rx} \times CL}}$$

This expression becomes our presented Eq. (3) and Eq. (4), when our measured data is captured in dB, dBi and/or dBm.

$$d_r = \frac{\lambda}{4\pi \times 10^{-C/40}}$$

and where

$$C = P_{tx} - P_{rx} + G_{tx} + G_{rx} - CL - 6.$$

Note that as the device's conversion loss, CL, is dependent on the incident power at the device, one will need to find d_r through iteration, as is outlined below:

1. Set initial d_r^n estimate, $n = 0$
2. Calculate $FSL_f(d_r)$ according to Eq. (8)
3. Calculate $P_{inc} = P_{tx} + G_{tx} - FSL_f$ (dBm, dBi, dB)
4. From prior data, find $CL(P_{inc})$
5. Insert new CL value into Eq. (3) to calculate new d_r^{n+1}
6. Repeat *Steps* $2 - 5$ until $d_r^{n+1} - d_r^n < \varepsilon$

ACKNOWLEDGMENT

The authors wish to thank the Fulbright Scholars Program and the Czech Fulbright Commission for making this collaboration possible. In addition, they wish to thank Václav Kabourek for preparing the test facilities utilized in this work.

REFERENCES

[1] D. Mascanzoni and H. Wallin, "The harmonic radar: A new method of tracing insect in the field," *Ecol. Entomol.*, vol. 11, no. 4, pp. 387–390, Nov. 1986.

[2] J. Roland, G. McKinnon, C. Backhouse, and P. D. Taylor, "Even smaller radar tags on insects," *Nature*, vol. 381, p. 120, May 1996.

[3] B. Colpitts and G. Boiteau, "Harmonic radar transceiver design: Miniature tags for insect tracking," *IEEE Trans. Antennas Propag.*, vol. 52, no. 11, pp. 2825–2832, Nov. 2004.

[4] R. Maggiora, M. Saccani, D. Milanesio, and M. Porporato, "An innovative harmonic radar to track flying insects: The case of Vespa velutina," *Sci. Rep.*, vol. 9, Aug. 2019, Art. no. 11964.

[5] J. Shefer and R. J. Klensch, "Harmonic radar helps autos avoid collisions," *IEEE Spectr.*, vol. 10, no. 5, pp. 38–45, May 1973.

[6] M. Ghazali, S. Karuppuswami, and P. Chahal, "3-D printed embedded passive harmonic sensor tag as markers for buried assets localization," *IEEE Sensor Lett.*, vol. 3, no. 4, pp. 1–4, Apr. 2019.

[7] H. Kwun, G. Burkhardt, and J. Fisher, "Detection of reinforcing steel corrosion in concrete structures using non-linear harmonic and intermodulation wave generation," U.S. Patent 5 180 969, 1993.

[8] V. Palazzi, F. Alimenti, P. Mezzanotte, G. Orecchini, and L. Roselli, "Zero-power, long-range, ultra low-cost harmonic wireless sensors for massively distributed monitoring of cracked walls," in *Proc. IEEE MTT-S Int. Microw. Symp. Dig.*, 2017, pp. 1335–1338.

[9] I. Uluer, J. Frolik, and T. Weller, "Battery-free mechanically-tunable wireless sensors for railroad track ballast monitoring," in *Proc. IEEE Symp. Antennas Propagat.*, 2022, pp. 117–118.

[10] B. Kubina, J. Romeu, C. Mandel, M. Schüßler, and R. Jakoby, "Design of a quasi-chipless harmonic radar sensor for ambient temperature sensing," in *Proc. IEEE Sensors*, 2014, pp. 1567–1570.

[11] X. Gu, S. Hemour, and K. Wu, "Improving conversion loss performance of fully passive harmonic transponder at low temperature," in *Proc. IEEE Wireless Power Transfer Conf.*, 2019, pp. 395–398.

[12] T. Silveira, P. Pinho, and N. Carvalho, "Harmonic RFID temperature sensor design for harsh environments," *IEEE Microw. Wireless Compon. Lett.*, vol. 32, no. 10, pp. 1239–1242, Oct. 2022.

[13] A. Lazaro, R. Villarino, and D. Girbau, "A passive harmonic tag for humidity sensing," *Int. J. Antennas Propagat.*, vol. 2, pp. 1–11, Jul. 2014.

[14] J. Frolik, J. Lens, M. Dewoolkar, and T. Weller, "Effects of soil characteristics on passive wireless sensor interrogation," *IEEE Sensors J.*, vol. 18, no. 8, pp. 3454–3460, Apr. 2018.

[15] G. L. Charvat, E. J. Rothwell, and L. C. Kempel, "Harmonic radar tag measurement and characterization," in *Proc. IEEE Antennas Propagat. Soc. Int. Symp. Dig.*, 2003, pp. 696–699.

[16] M. Polivka, V. Hubata-Vacek, and M. Svanda, "Harmonic balance / full-wave analysis of wearable harmonic transponder for IoT applications," *IEEE Trans. Antennas Propag.*, vol. 70, no. 2, pp. 977–987, Feb. 2022.

[17] R. O. Hstger, "Harmonic radar systems for near-ground in-foliage nonlinear scatterers," *IEEE Trans. Aerosp. Electron. Syst.*, vol. 12, no. 2, pp. 230–235, Mar. 1976.

[18] K. Rasilainen, J. Ilvonen, A. Lehtovuori, J.-M. Hannula, and V. Viikari, "On design and evaluation of harmonic transponders," *IEEE Trans. Antennas Propag.*, vol. 63, no. 1, pp. 15–23, Jan. 2015.

[19] J.-M. Hannula, K. Rasilainen, and V. Viikari, "Characterization of transponder antennas using intermodulation response," *IEEE Trans. Antennas Propag.*, vol. 63, no. 6, pp. 2412–2420, Jun. 2015.

[20] X. Gu, N. Srinaga, L. Guo, S. Hemour, and K. Wu, "Diplexer-based fully passive harmonic transponder for sub-6-GHz 5G-compatible IoT applications," *IEEE Trans. Microw. Theory Tech.*, vol. 67, no. 5, pp. 1675–1687, May 2019.

[21] A. D. Yaghjian and S. R. Best, "Impedance, bandwidth, and Q of antennas," *IEEE Trans. Antennas Propag.*, vol. 53, no. 4, pp. 1298–1324, Apr. 2005.

[22] I. T. Nassar, J. Wang, J. L. Frolik, and T. M. Weller, "A high-efficiency, miniaturized sensor node with 3-D machined-substrate antennas for embedded wireless monitoring," *IEEE Sensors J.*, vol. 15, no. 9, pp. 5036–5044, Sep. 2015.

[23] K. Gumber, C. Dejous, and S. Hemour, "Harmonic reflection amplifier for widespread backscatter Internet-of-Things," *IEEE Trans. Microw. Theory Techn.*, vol. 69, no. 1, pp. 774–785, Jan. 2021.

[24] T. Rappaport, *Wireless Communications, Principles and Practice*, 2nd ed., Hoboken, NJ, USA: Prentice Hall, 2002.

[25] M. Polivka and J. Frolik, "Characterizing harmonic transponder performance jointly over frequency and power," in *Proc. Eur. Conf. Antennas Propagat.*, 2023, pp. 1–5.

[26] C. Cho, X. Yi, D. Li, Y. Wang, and M. M. Tentzeris, "Passive wireless frequency doubling antenna sensor for strain and crack sensing," *IEEE Sensors J.*, vol. 16, no. 14, pp. 5725–5733, Jul. 2016.

[27] (RF Spin, Prague, Czechia), "Quad Ridged Horn Antenna," (2022). [Online]. Available: https://www.rfspin.com/product/qrh11/

[28] "Surface mount RF Schottky barrier diodes", AV02-1320EN, AVAGO Technol., San Jose, CA, USA, May 2009.

[29] K. Rasilainen and V. Viikari, "Transponder designs for harmonic radar applications," *Int. J. of Antennas Propagat.*, vol. 4, pp. 1–9, Sep. 2015.

[30] (RECCO AB, Lidingö, Sweden) "RECCO reflector," Accessed: Nov. 23, 2023. [Online]. Available: https:www.recco.com

[31] J. Frolik and M. Polivka, "Impact of bodies on harmonic transponder conversion loss and radiation patterns," *IEEE Antenna Propagat. Symp.*, 2023, pp. 1339–1340.

[32] L. Zhu, H. Huang, M. M.-C. Cheng, and P.-Y. Chen, "Compact, flexible harmonic transponder sensor with multiplexed sensing capabilities for rapid, contactless microfluidic diagnosis," *IEEE Trans. Microw. Theory Tech.*, vol. 68, no. 11, pp. 4846–4854, Nov. 2020.

MILAN POLIVKA (Member, IEEE) received the M.S. and Ph.D. degrees in radioelectronics from the Czech Technical University (CTU), Prague, Czech Republic, in 1996 and 2003, respectively.

Since 2013, he has been an Associate Professor with the Faculty of Electrical Engineering, CTU, where he has also been the Vice Dean for Doctoral Studies and Science since 2015. From 2003 to 2014, he was a Co-Founder of the startup RFspin. He has authored or coauthored of more than 100 papers published in international journals or conference proceedings. His current research interests include antennas, microwave technique, and applied electromagnetism.

Dr. Polivka was the Chairman of the Czechoslovak Section of IEEE from 2010 to 2011.

JEFF FROLIK (Senior Member, IEEE) received the B.S. degree in electrical engineering from the University of South Alabama in 1986, the M.S. degree in electrical engineering from the University of Southern California in 1988, and the Ph.D. degree in electrical engineering systems from the University of Michigan in 1995.

From 1986 to 1995, he was a Satellite Systems Engineer with the Hughes Aircraft Company. From 1995 to 1998, he was an independent consultant in the area of satellite communications. From 1998 to 2002, he was an Assistant Professor with Tennessee Technological University. Since 2002, he has been with the University of Vermont, where he is currently a Professor of Electrical Engineering. From 2016 to 2021, he was a co-founder of the startup Packetized Energy. His areas of research are sensor networks and wireless propagation.